

Correlation of Local Constitutive Properties to Global Mechanical Performance of Advanced High-Strength Steel Spot Welds



H. REZAYAT, H. GHASSEMI-ARMAKI, S. SRIRAM, and S.S. BABU

Recent results have shown that the strength of resistance spot-welded joints made from advanced high-strength steels (AHSS) do not increase linearly with their base metal strength. While the martensite tempering and subsequent softening in a narrow heat affected zone (HAZ) of these joints has been reported as a primary cause for this degradation, the quantitative effects of HAZ softening on above nonlinearity in different steels have not been explored. In this research, the role of material heterogeneity on load-displacement characteristics of dual-phase and martensitic AHSS with initial martensite volume fractions of 16, 58, and 100 pct during tension-shear (TS) and cross-tension (CT) testing was modeled with finite element method and compared with experimental measurements of global deformation and fracture behavior. Results from low-strength steels showed that the location of HAZ failure transitions from hardened to softened regions, as the nugget diameter increases from 4 to 6 and 8 mm, even with the presence of softening in the HAZ. At the same time, the results from higher strength steels showed more sensitivity to the softened region in larger nugget diameters. This result elucidates that the nonlinearity in strength of high-strength AHSS spot welds in comparison to lower strength of mild steel, is due to their intrinsic brittleness, as well as the overall geometry of the weld nugget. Our results also suggest that, while HAZ softening plays a detrimental role in DP steels, it helps to improve the ultimate load and global extension in high strength grades. Finally, several uncertainties related to finite element simulations and experiments have been highlighted. The results from this study can help in optimizing the resistance spot-welding process parameters and the design of the part made from AHSS.

<https://doi.org/10.1007/s11661-020-05714-3>

© The Minerals, Metals & Materials Society and ASM International 2020

I. INTRODUCTION

RECENT results from researchers have shown that spot welds in dual-phase and martensitic advanced high-strength steels exhibit softening and hardening in their heat-affected zone. These phenomena are found to be a function of martensite fraction and carbon content.^[1,2] Results from mechanical testing on tension-shear and cross-tension welded samples with different nugget diameters (ND) show nonlinear relationship between the strength of base metal (BM) and maximum load from tension-shear and cross-tension

spot welds.^[3,4] This nonlinearity can potentially impact the expected performance of AHSS spot welds, during the design of components with reduced weight and improved crashworthiness.

With the onset of new regulations for the automotive industry on emissions, steel makers have been designing and producing a class of steels known as advanced high strength steels (AHSS) to reduce the weight and fuel consumption and increase the safety of cars. Dual-phase (DP) and Martensitic (MS) steels are among the AHSS that are widely used in manufacturing of chassis and body structure of the automobile. Resistance Spot welding (RSW) is the main joining technique in manufacturing of the components made from these steels. DP and MS steels have a ferritic-martensitic and fully martensitic microstructures, respectively. Although martensite is a hard microconstituent with high levels of tensile strength (up to about 2800 MPa), it has a metastable structure and decomposes into ferrite and carbide during RSW.^[1,2,5-8] This phenomenon known as martensite tempering, occurs at temperatures below the A_{e1} phase transformation temperature of steel, and has been extensively studied by several researchers, text

H. REZAYAT is with the Mechanical, Aerospace and Biomedical Engineering, University of Tennessee, Knoxville, TN. Contact e-mail: hrezayat@vols.utk.edu H. GHASSEMI-ARMAKI and S. SRIRAM are with the Automotive Product Research, ArcelorMittal Global R&D, East Chicago, IN. S.S. BABU is with the Mechanical, Aerospace and Biomedical Engineering, University of Tennessee and also with the Manufacturing Demonstration Facility, Oak Ridge National Laboratory, Oak Ridge, TN.

Manuscript submitted July 10, 2019.

Article published online March 10, 2020

books and standards.^[4,5,9–13] Many of the published results also show that constitutive properties of these steels may be heterogeneous within the spot welds, depending on the initial microstructure and carbon content.^[1,2,4,6,12,14,15] In general, HAZ softening has been observed in both intercritical HAZ (ICHAZ) (due to formation of fresh ferrite) and subcritical HAZ (SCHAZ) (due to tempering of martensite) of resistance spot welds, made from the DP and MS advanced high strength steels, with different extents depending on the initial microstructure and chemical composition. This leads to some fundamental questions regarding the effects of these gradients on the deformation and failure behavior of the spot welds. The deformation and failure modes of the spot-welded samples had been investigated before.^[4,16–27] The effects on discontinuous yielding in the form of yield point phenomena on deformation and failure behavior of AHSS spot welds has also been investigated in literature^[28] and in this work it is assumed that this phenomena does not affect the mechanical performance of spot welds. The literature suggests that the strength and failure in spot welds is a function of both geometry of the spot weld and material properties.^[4,17,18,20–22,29,30] In these studies, failure mode of spot welds has been classified into two main types of failures, *i.e.*, (i) interfacial failure (IF) and (ii) round button (RB, also known as plug failure (PF)). In interfacial failure, crack propagates through the nugget of the weld on the faying surface of spot weld (fully interfacial failure, FIF), or initially moves on the faying surface and then deviates through the thickness of steel sheet and passes through the FGHAZ and/or CGHAZ. The second type of failure, *i.e.*, RB failure, can take place in two regions of HAZ: (i) in softened HAZ (ICHAZ and SCHAZ), termed RBH, and (ii) in fine-grained HAZ (FGHAZ) and coarse-grained HAZ (CGHAZ), termed RB. The two FGHAZ and CGHAZ belong to the upper-critical HAZ (UCHAZ) where the peak temperature during the resistance welding process reaches to values above A_{e3} phase transformation and melting temperatures of the steel. A combination of above failure modes can also occur in AHSS spot welds.

While the role of spot weld geometry on the strength and failure of spot-welded samples have been studied extensively, the individual roles of weld geometry and HAZ softening have not been explored comprehensively. In this paper, the local constitutive properties obtained from tensile testing and digital image correlation on Gleeble-simulated HAZ samples are used as material input for finite element (FE) simulations. Our motivation is that these descriptive FE simulations will provide insight to understand the local-global deformation and failure relationship in resistance spot welds made from DP and MS AHSS.

II. EXPERIMENTAL PROCEDURE

A. Materials

Three grades of AHSS including DP590, DP980LC, and M1700 were used in this study. Chemical composition, initial microstructure and tensile properties for

these steels are shown in Tables I and II, for comparison. As can be seen, these three steel grades represent a wide range of carbon content and martensite volume fraction in the base metal. This enabled us to understand the role of initial microstructure and chemistry on the mechanical performance of the final spot-welded tension-shear and cross-tension samples. Uniaxial tensile testing was used in concert with ASTM E8 standard^[31] to evaluate the as-received mechanical properties. The volume fraction of martensite in base metal of DP steels was calculated by image processing of the micrographs obtained from optical microscopy of samples etched using Nital 2 pct. ASTM E3^[32] standard was used for preparation of metallographic samples were needed. Martensite volume fraction and its partitioned carbon content in equilibrium condition are denoted by f_M and C_M , respectively. Mass spectrometry was used to obtain chemical composition of steels.

B. Local Constitutive Properties and Damage Model

The local thermal cycles from the resistance spot-welding process result in heterogeneous constitutive properties within DP and MS AHSS spot welds. To understand the local-global deformation and failure behavior in spot welds there is a need for local constitutive properties as material input in FE simulations. In this study, these local mechanical properties (true stress vs strain curves) were extracted from our previous research^[1] involving tensile testing and digital image correlation (DIC) technique. The DIC equipment was manufactured by Correlation Solutions[®] and the VIC-2D post-processing software, was used for this purpose. The engineering stress-strain curves for BM and HAZ of DP590, DP980LC, and M1700 evaluated in our previous study^[1] are shown in Figures 1(a) through (c), respectively.

To simulate the damage initiation, propagation, and failure of the TS and CT samples, the ductile damage model provided by Abaqus software (details can be seen here^[33]) was used in all FE simulations. This damage model assumes that the equivalent plastic strain at the onset of damage is a function of stress triaxiality and strain rate, however, in this work due to several number of parameters (material, nugget diameter, HAZ regions, sample type) it was assumed that failure criteria is independent of stress triaxiality and/or strain rate. Therefore, a constant value was used for each region of weld in the FE simulations. To obtain

Table I. Chemical Composition, Martensite Volume Fraction and Its Partitioned Carbon Content for the Investigated AHSS Used in This Study

Steel	Alloying Elements (Wt Pct)			C_M (Wt Pct)	f_M (Vol Pct)
	C	Mn	Si		
DP590	0.09	0.99	0.28	0.44	16
DP980LC	0.10	2.19	0.65	0.15	59
M1700	0.31	0.47	0.19	0.31	100

the equivalent plastic strain at failure for each region of HAZ, a virtual extensometer with a length of 1 mm was in the strain measurements from DIC data. This was the smallest possible extensometer relevant to DIC analysis based on the dimensions of the sample and experimental setup. The same material properties were used for the nugget and FGHAZ-1250 °C as it was not practical to reproduce molten region in Gleeble thermo-physical simulator. The plastic strains at failure for different regions of HAZ and base metal for spot welds made from the three steels of this study are presented in Table III.

C. Welding Equipment and Overview of Mechanical Tests

Uniaxial tensile (UT) tests were performed according to ASTM E8^[31] on base metal samples to obtain the as-received mechanical properties as reported in Table II. Tension-shear (TS) and cross-tension (CT)

samples were prepared by welding two sheets of the same steel and using welding parameters that resulted in nugget diameters of 4, 6, and 8 mm. The geometry of above samples and mechanical tests procedure were adopted from the AWS D8.9 standard.^[34] A Taylor-Winfield 75–85 kVA resistance welding machine with 60 HZ single-phase AC current was used for welding TS and CT samples. Type A 16 mm ISO 6.0 mm EFD electrodes were used with a water cooling system and 6 L/min water flow. Resistance spot welding procedure sequence included 70 cycles for squeezing steel sheets, two pulses of 12 cycles as weld time, cooling step of 2 cycles between the two welding pulses and hold time of 10 cycles. A constant electrode load of 5 kN was used for all spot welds. An MTS Criterion C45 tensile frame with constant displacement rate of 2 mm/min was used for all mechanical tests and results were recorded in the form of load-extension for comparison with those from FE simulations.

Table II. As-Received Tensile Properties for the Three AHSS Grades Used in this Study

Steel	Thickness (mm)	YS (MPa)	UTS (MPa)	Total Elongation (Pct) (25-mm Gauge Length)
DP590	1.5	390	636	23
DP980LC	1.4	710	1056	13
M1700	1.6	1706	1876	5

Uniaxial Tensile Testing was Used to Obtain These Properties Following ASTM E8 Standard.

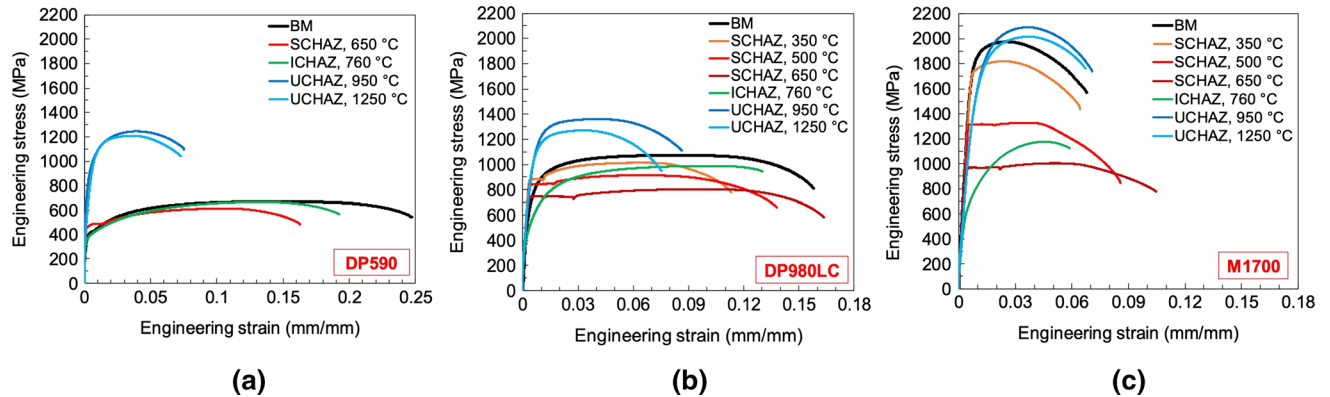


Fig. 1—Local constitutive properties in the form of engineering stress–strain curves obtained from integrated uniaxial tensile testing and digital image correlation technique performed on base metal and Gleeble simulated HAZ uniaxial tensile samples made from for DP590 (a), DP980LC (b), and M1700 (c). Reprinted by permission from Ref. [1].

Table III. Equivalent Plastic Strain at Failure for Different Regions (Peak Temperatures in Gleeble Simulations) of HAZ for Three Grades of AHSS Used in This Study

Steel	SCHAZ-350 °C	SCHAZ-500 °C	SCHAZ-650 °C	ICHAZ-760 °C	FGHAZ-950 °C	CGHAZ-1250 °C
DP590	—	—	0.95	0.86	0.08	0.06
DP980LC	0.61	0.68	0.72	0.45	0.07	0.06
M1700	0.46	0.64	0.61	0.34	0.07	0.05

III. FINITE ELEMENT SIMULATIONS

A. Geometry modeling

Three-dimensional FE models for the TS and CT samples were prepared in Abaqus commercial FE package by following the specifications detailed in AWS D8.9 standard.^[35] Only half of TS and one quarter of CT samples were modeled, due to the symmetrical geometry and for sake of reduction in computational time. These models are shown in Figure 2. To investigate the role of individual weld zones in deformation and failure behavior of AHSS spot welds and due to strong material heterogeneity in HAZ, as illustrated in Figure 3, these FE models were partitioned into several regions including base metal (BM), SCHAZ-350 °C, SCHAZ-500 °C, SCHAZ-650 °C, ICHAZ-760 °C, UCHAZ-950 °C, UCHAZ-1250 °C, and fusion zone or nugget (FZ). This partitioning was done based on the number of peak temperatures that were used in Gleeble simulations as detailed in a previous work^[1] by the authors of this paper. It needs to be mentioned that the geometry (especially the width of weld zones) was determined using the results from microstructural analysis using scanning electron microscopy (SEM) and also microhardness maps, as shown in Figure 3.

B. Mesh Design and Choice of FE Solver

Mesh design was performed for UT, TS, and CT finite-element models by considering the complexity of geometry, local material mechanical properties, and expected local deformations. Special attention was given to the ICHAZ of spot welds as it is a very narrow region with a typical width of about 200 μm (depending on the distance between the Ae_1 and Ae_3 phase transformation temperatures of steel) and bridges SCHAZ and FGHAZ with a sharp transition in material mechanical properties, from softened to hardened HAZ. Continuum three-dimensional hexahedral elements with reduced integration scheme were used in all the FE models.

Because of the complex geometry of the spot welds, large plastic deformations, nonlinear elastic–plastic constitutive properties, and the use of progressive damage model with element removal technique for prediction of crack initiation, growth and failure, the explicit FE solver was used in this study. It has to be mentioned that the implicit solver was able to predict the deformation behavior up to the damage initiation point however it was not able to complete the simulations due to above reasons, and therefore, the explicit solver was used in all the FE simulations of this study. To reduce the computational time, mass and time-scaling techniques were used in all the FE simulations.

IV. RESULTS

A. Global Deformation and Failure Behavior

Results from FE simulations and experiments performed on TS and CT samples with nugget diameters of 4, 6, and 8 mm made from three steels of this study are presented in Figure 4. Failure modes from FE models and experiments are also reported in the same figure. It has to be noted that these results are normalized with the thickness of the steel sheet. As can be seen, there are differences between peak load and global extension values obtained from FE simulations and those from experiments. This can be explained by considering several uncertainties that may exist in the results from both the FE simulations and experiments. An overview on these uncertainties is brought later in this paper. However, these results are comparable and FE models for TS and CT samples were able to predict the deformation behavior and failure modes for the samples in global and local terms.

The performance of the spot welds can be studied as a function of two main parameters: (1) spot weld geometry, here the nugget diameter (ND), and (2) steel's chemical composition and initial microstructure which govern the constitutive properties, here base metal strength (BMS). Figure 5 compares the strength (peak

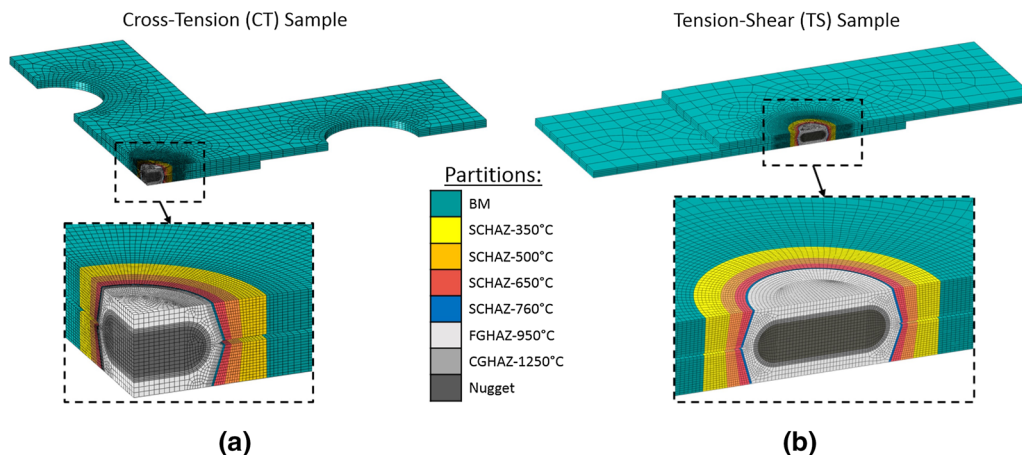


Fig. 2—Finite element models for CT (a) and TS (b) samples with partitioned HAZ, material assignment, and mesh design. Due to the symmetrical geometry and for the sake of computational time only one fourth and a half of the CT and TS samples were modeled, respectively.

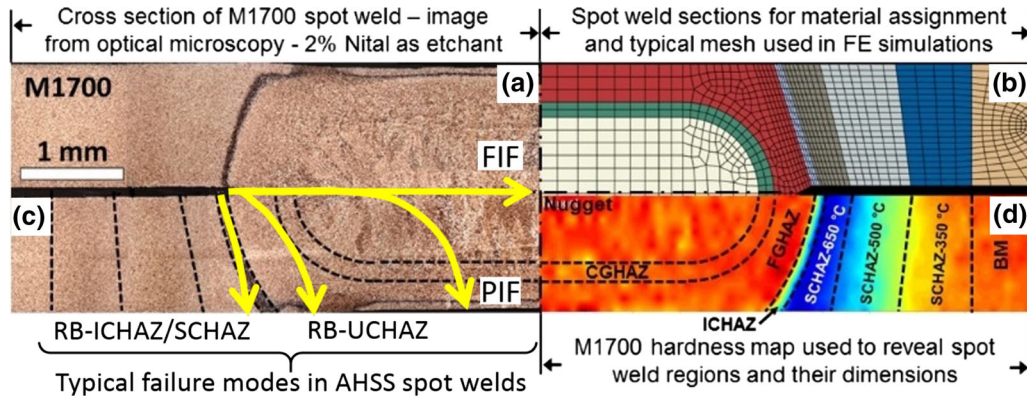


Fig. 3—Cross-section of M1700 spot weld demonstrating: micrograph from Nital 2 pct-etched cross-section obtained from scanning electron microscopy analysis (a), demonstration of the FE model with partitioned and meshed HAZ (b), typical failure location and modes in AHSS spot welds (c) and hardness map (d). Reprinted by permission from Ref. [28].

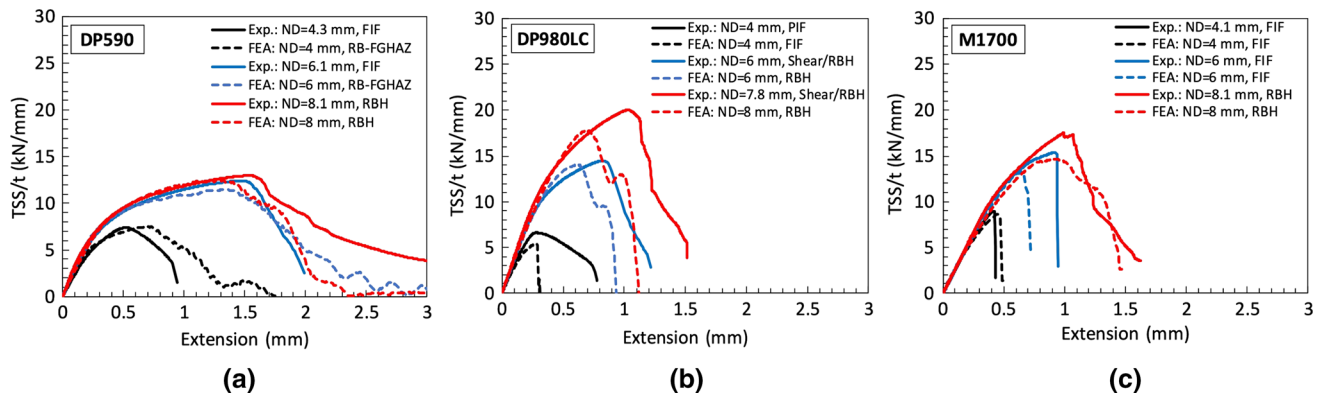


Fig. 4—Results from experiments and FE simulations for DP590 (a), DP980LC (b), and M1700 (c) tension-shear samples with 4, 6, and 8 mm nugget diameters. Failure modes are also shown for comparisons. FE models were able to predict the deformation behavior and failure modes.

load) of TS (TSS) and CT (CTS) spot-welded samples as functions of ND and BMS. These results, in general, show an initial increase in TSS and CTS with ND and/or BMS and then an unexpected decrease in the slope of the plots as ND and BMS pass 6 mm and 980 MPa (corresponding to DP980LC steel), respectively. As there are only three nugget diameters used in this study, we use the 6 mm nugget diameter as the critical value, ND_{cr} , for the rest of this study. However, the exact value for the nugget diameter can be smaller or larger than this value. We also use the BMS_{cr} as the critical value among the three steels of this study, however, there might be other grades of steels not used in this study that have the critical value for BMS.

From Figures 5(a) and (c), the effect of nugget diameter on TSS and CTS can be observed. In general, increase in nugget diameter leads to increase in TSS and CTS, however, its effectiveness decreases as the nugget diameter passes the critical value, 6 mm to be used in this study. One interesting observation is that, in general, the failure mode changes above the critical ND and BMS, from the IF or RB-UHAZ (also called shear and RB) in the martensitic (hardened) HAZ to RB-ICHAZ/SCHAZ (also RBH) in the softened HAZ with DP ferritic/martensitic microstructure in ICHAZ

and tempered martensite in SCHAZ. For the CT samples, a change in failure mode from RB to RBH is clear in all samples. On exemption from this general trend is the experimental result for TSS of DP980LC sample for which the strength continuously increases without any drop. For this sample, results from FE simulations showed no change in failure mode by passing the nugget diameter of 6 mm, which is in contrast with results from the experiments that showed RBH failure. This result is tentatively attributed to the uncertainties in data and testing methodologies and will be discussed later.

The strength of the spot welds can also be plotted as a function of their base metal strength, BMS. This is shown in Figures 5(b) and (d) for all the nugget diameters. In these two plots and for both TSS and CTS, the nonlinearity increases with nugget diameter, indicating the role of weld geometry on the nonlinearity in strength of AHSS spot welds.

B. Plastic Strain Localization and Failure Modes

Figure 6 shows the equivalent plastic strain localization, crack initiation and propagation, and failure on cross-section of TS samples with three different nugget

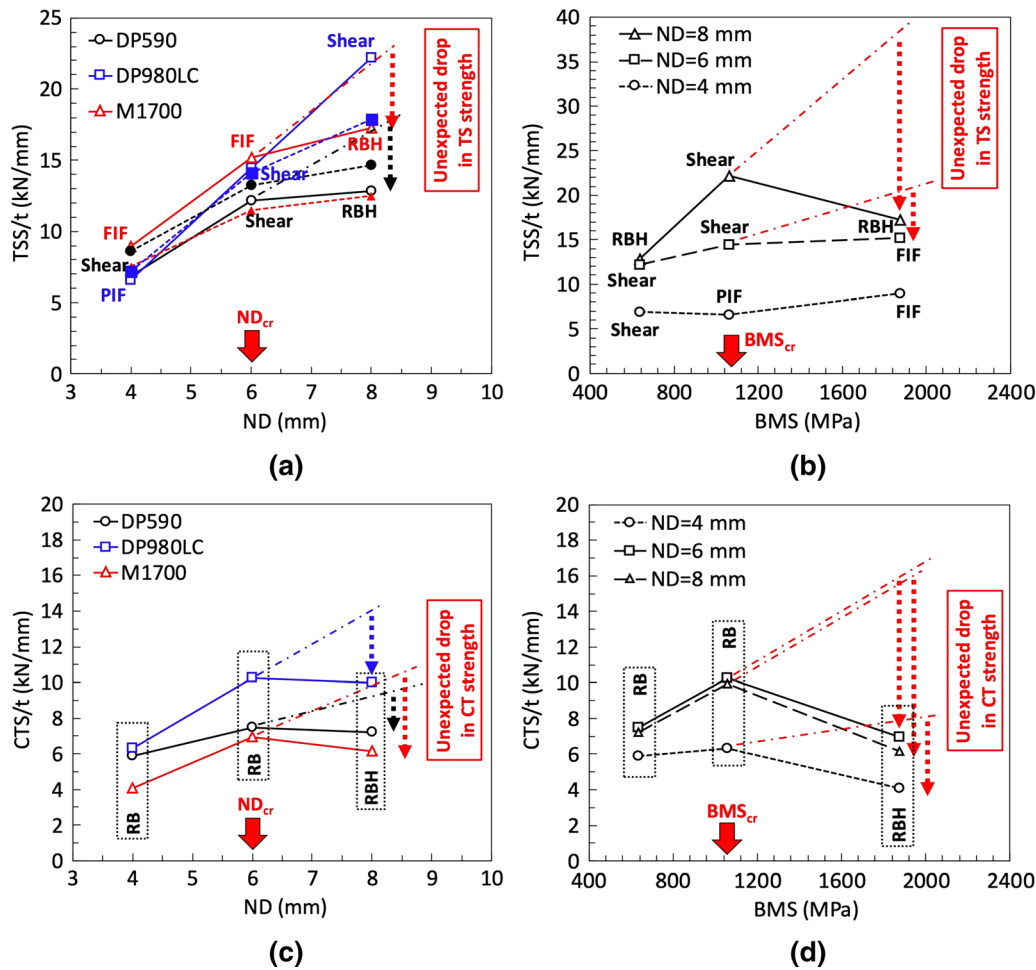


Fig. 5—Experimental results from TS (a) and (b), and CT (c) and (d) samples made from DP590, DP980LC, and M1700 steels with three nugget diameters of 4, 6, and 8 mm. The initial martensite volume fraction for these steels are 16, 59, and 100 percent, respectively. Failure mode for each sample is also shown.

diameters made from M1700. From this figure three different failure modes can be distinguished. For the nugget diameter of 4 and 6 mm although the initial plastic strain localization occurs in the ICHAZ (with the lowest yield stress in entire sample), the loading condition and rotation of the sample around the center of nugget promotes the accumulation of plastic strain in the notch tip of the spot weld and by increase in the global loading, the equivalent plastic strain at this region elevates up to the local plastic strain failure criteria and consequently damage (crack) initiates at this point. The increase in the global loading or extension results in rapid crack propagation in the faying surface of the nugget and eventually sample fails with FIF failure mode. Results shown in Figure 4 show brittle failure mechanism that occurs in this region with martensitic microstructure. For the nugget diameter of 6 mm, the plastic strain localization and failure take place in the regions above the Ae_3 phase transformation temperature, corresponding to the FGHAZ and CGHAZ, based on results from FE simulations and experiments. An RB-FGHAZ/(CGHAZ) failure mode can be expected for the welds with this nugget diameter. The local microstructure in this region is also mainly

martensitic^[1] and a semi-brittle failure mechanism can be expected. For the TS sample with 8 mm nugget diameter, the plastic strain localization, crack initiation, and failure take place in the ICHAZ resulting in RB-ICHAZ (RBH) failure mode. The local material behavior in this region is dual-phase ferritic-martensitic^[1] and a ductile failure mechanism can be expected. For the RB-ICHAZ there have been cases that the crack deviated from the ICHAZ to the SCHAZ, and therefore, an RB-ICHAZ/SCHAZ can also be considered. Results from previous study^[1] showed that the local microstructure in this region consists of tempered martensite and ferrite (in dual-phase steels). Similar behavior was observed in FE simulations of other steels used in this study, DP590 and DP980LC and validated by the results from TS and CT experiments.

V. DISCUSSION

Results presented in previous section reconfirmed that the strength of TS and Ct samples (TSS and CTS, respectively) does not increase linearly with ND and BMS. This is very important from the end users'

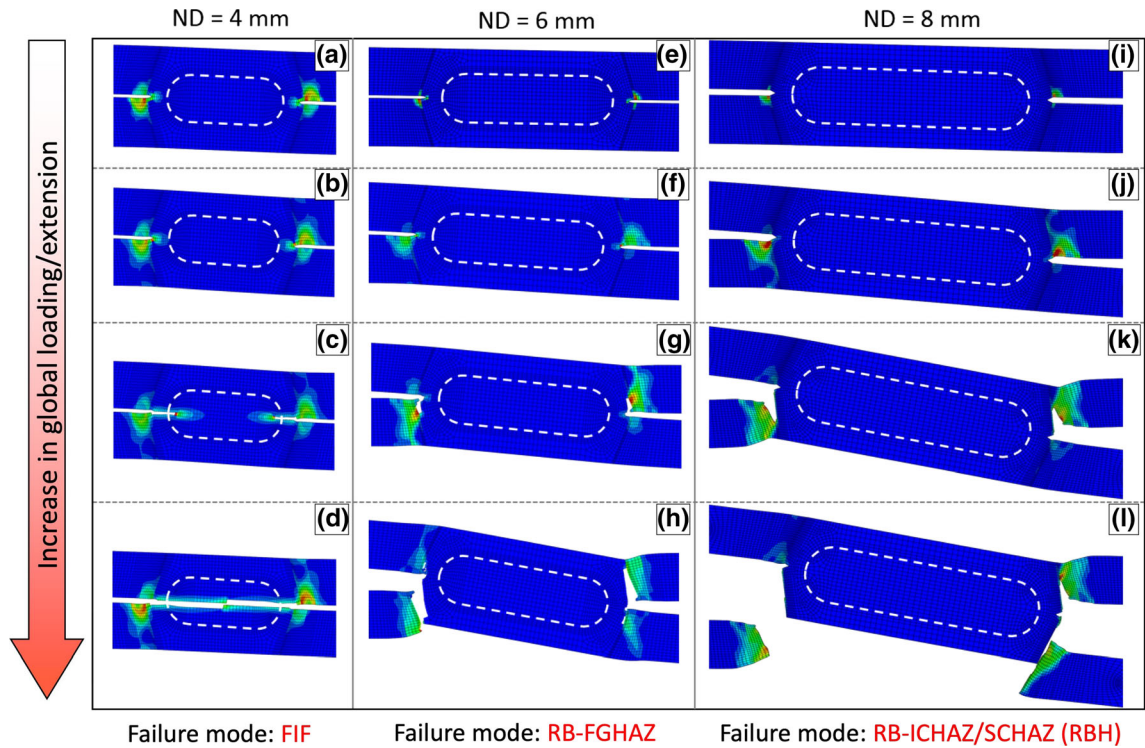


Fig. 6—Results from FE simulation of TS test for M1700 spot welds with 4, 6, and 8 mm nugget diameters. The evolution and localization of the equivalent plastic strain on the cross-section of samples can be seen. Three failure modes were observed: FIF for ND = 4 mm (a) through (d), RB-FGHAZ for ND = 6 mm (e) through (h), and RB-ICHAZ for ND = 8 mm (i) through (l). The main competition was observed between the ICHAZ and FGHAZ based on the strain localization, crack initiation, propagation, and failure.

perspective, especially in automotive industry. End-use customers expect to see increase in strength of AHSS spot welds by increase in ND and/or BMS. More importantly, the goal of developing AHSS with higher tensile strength is to improve the performance and safety of parts, for example in automotive industry, made from these steels, and the nonlinear behavior is against this goal. Therefore, we need to understand the underlying phenomena that result in this nonlinearity and suggest methods to resolve this issue. This is the goal of this paper.

Results presented in previous section reconfirmed the existence of a nonlinear relationship between the base metal strength and the strength of tension-shear and cross-tension samples made from AHSS of this study. Nugget diameter (geometrical factor) and base metal tensile strength (related to the chemical composition and initial microstructure of steels) both showed to have direct impact on the strength and failure behavior of AHSS spot welds of this study, and failure mode showed significant change as nugget diameter increased in majority of cases. In this section results from experiments and FE simulations are used to explain the above nonlinearity by considering the individual role of nugget diameter and material heterogeneity, with particular attention to the HAZ softening that occurs in both

ICHAZ and SCHAZ of AHSS DP and MS steels. Local and global evaluations will be used to explain the nonlinearity in the strength of these welds.

A. Role of HAZ Softening on Performance of Spot Welds

FE simulations were used as a tool to investigate the role of HAZ softening (occurring in ICHAZ and SCHAZ) on mechanical performance of TS and CT samples. FE models for TS and CT samples with 8 mm nugget diameter and M1700 steel were selected for this study. The selection of grade of steel and nugget diameter was based on two facts: (i) the largest extent of softening was observed in this steel based on hardness measurements from previous study,^[1] and (ii) results from TS and CT experiments presented in Figure 5 showed that the highest degradation in TSS and CTS belongs to spot welds with nugget diameter of 8 mm. The methodology for this investigation is based on substituting the material properties of certain softened regions (ICHAZ and/or SCHAZ) in the FE models for TS and CT samples with that of base metal or adjacent region, simulating the condition that the HAZ softening does not occur in these two regions. Based on this methodology, following cases (also shown in Table IV) were considered in this study:

Table IV. Material Assignment to Different Regions of the Spot Weld for Studying the Role of HAZ Softening on Spot Weld Performance

		Material Properties Assigned to HAZ of TS and CT Samples (ND = 8 mm)																
Case I	CGHAZ-1250 °C	CGHAZ-1250 °C	CGHAZ-1250 °C	FGHAZ-950 °C	ICHAZ-760 °C	SCHAZ-650 °C	SCHAZ-500 °C	SCHAZ-350 °C	BM	CGHAZ-1250 °C	CGHAZ-1250 °C	CGHAZ-1250 °C	FGHAZ-950 °C	ICHAZ-760 °C	SCHAZ-650 °C	SCHAZ-500 °C	SCHAZ-350 °C	BM
Case II	CGHAZ-1250 °C	CGHAZ-1250 °C	CGHAZ-1250 °C	FGHAZ-950 °C	SCHAZ-650 °C	SCHAZ-650 °C	SCHAZ-500 °C	SCHAZ-350 °C	BM	CGHAZ-1250 °C	CGHAZ-1250 °C	CGHAZ-1250 °C	FGHAZ-950 °C	ICHAZ-760 °C	SCHAZ-650 °C	SCHAZ-500 °C	SCHAZ-350 °C	BM
Case III	CGHAZ-1250 °C	CGHAZ-1250 °C	CGHAZ-1250 °C	FGHAZ-950 °C	ICHAZ-760 °C	BM	BM	BM	BM	CGHAZ-1250 °C	CGHAZ-1250 °C	CGHAZ-1250 °C	FGHAZ-950 °C	ICHAZ-760 °C	BM	BM	BM	BM
Case IV	CGHAZ-1250 °C	CGHAZ-1250 °C	CGHAZ-1250 °C	FGHAZ-950 °C	BM	BM	BM	BM	BM	CGHAZ-1250 °C	CGHAZ-1250 °C	CGHAZ-1250 °C	FGHAZ-950 °C	BM	BM	BM	BM	BM

1. Case I: The real spot weld with softening in both ICHAZ and SCHAZ regions.
2. Case II: Softening does not occur in ICHAZ (this region has the minimum yield stress throughout the spot weld) and material properties for SCHAZ-650 °C is used for this region.
3. Case III: Softening does not occur in SCHAZ (all three peak temperatures) and material properties for BM were used for these regions.
4. Case IV: Softening does not occur in the entire weld and BM material properties were used for both ICHAZ and SCHAZ.

TSS and CTS values obtained from FE simulations for cases shown in Table IV are presented in Figure 7, for comparisons. These results show that as the number of regions with softening increase the effect of softening on mechanical performance of TS and CT samples becomes more noticeable. While for Case II (samples without softening in ICHAZ) the change in TSS and CTS is about 0.2 and 4.1 pct, respectively, this change in strength (peak load) increases to 12.1 and 14.3 pct, respectively, for Case III (without any softening in HAZ). These results show that even by removing the entire HAZ softening (both SCHAZ and ICHAZ, Case IV) from the HAZ of TS and CT samples made from this grade of steel, the strength on spot-welded sample does not increase by more than about 15 pct, considering all cases. Therefore, it can be assumed that the softening is not a dominant factor in degradation of strength in martensitic (MS) AHSS steels and the geometry (nugget diameter) is the main factor.

Similar analysis was performed for DP980LC steel to understand if the same influence can be seen. The results from this analysis are combined with those for M1700 and presented in Figure 8, in form of global load-extension curves, for comparisons. Results are unexpected and show that HAZ softening has a completely different role in spot welds made from DP980LC when compared with M1700. While the role of HAZ softening was minor in M1700 spot weld performance, it significantly

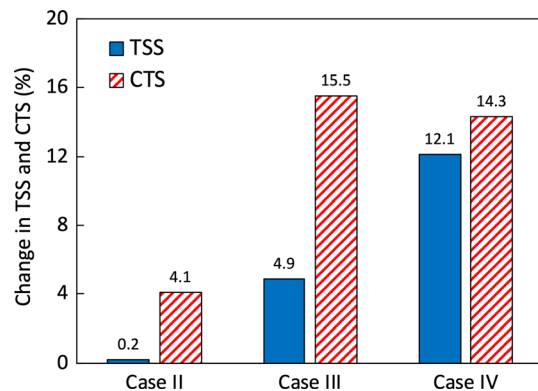


Fig. 7—The change in TSS and CTS when compared with as-weld FE model (Case I), when the softening in SCHAZ and/or ICHAZ were not included in FE simulations. Results show that exclusion of only ICHAZ has minimal impact on both TSS and CTS while the exclusion of SCHAZ (Case III) or both SCHAZ and ICHAZ (Case IV) can result in up to 15.5 pct change (increase) in TSS and CTS.

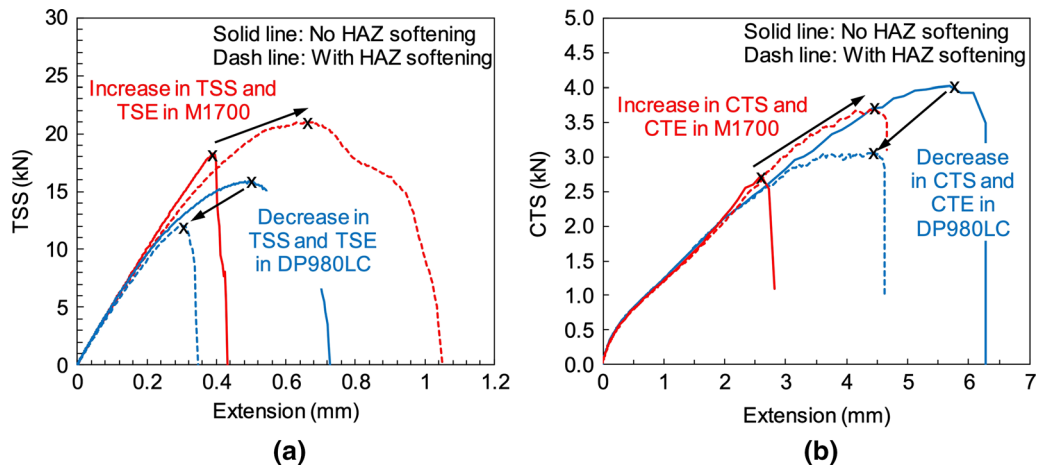


Fig. 8—The effect of HAZ softening on mechanical performance of TS (a) and CT (b) samples for DP980LC and M1700 steels showed that the role of HAZ softening is complex and different in different grades of AHSS. While HAZ softening deteriorates the performance of DP980LC spot welds it improves the performance of M1700.

impacts the strength (TSS and CTS) and extension at peak load (TSE and CTE for TS and CT samples, respectively) in samples made from DP980LC. For this steel, the HAZ softening decrease TSS and TSE by about 44 and 32 pct and CTS and CTE by about 31 and 36 pct, respectively. These changes for M1700 spot welds were about 12 and 42 pct increase in TSS and TSE, and 14 and 63 pct increase in CTS and CTE, respectively. Therefore, while HAZ softening has a positive impact on mechanical performance of M1700, it has a negative impact on DP980LC spot welds.

Results from FE simulations presented above for DP980LC and M1700 steels are combined with the experimental data for spot-welded samples made from a range of DP and MS AHSS and presented in Figure 9. In this figure, it is assumed that HAZ softening has a linear effect on the strength of spot welds made from DP and MS AHSS, meaning that the strength of spot welds increases linearly with the extent of softening in HAZ that has been shown to be related to initial microstructure and carbon content of steels.^[1,2,14,36] The effect of HAZ softening on mechanical performance of AHSS spot welds can be rationalized by considering the extent of HAZ softening and its role in local and global deformations in spot welds. As an example, in spot welds made from DP590 with 16 pct martensite in its base metal, the extent of HAZ softening is minor (with only about 6 pct drop in hardness in SCHAZ and/or ICHAZ^[1,2]), and therefore, a slight impact on the strength of spot welds (TSS and CTS) can be expected. This is shown in Figure 9 by a small difference between the values from tension-shear experiments and that without HAZ softening obtained from FE simulations. For spot welds made from DP980LC we can see the maximum effect in the form of reduction in strength of spot weld. This DP steel has about 59 pct martensite in its initial microstructure and has shown a higher extent of softening in HAZ (18 pct drop in hardness in SCHAZ and/or ICHAZ, from References 1 and 2) and results

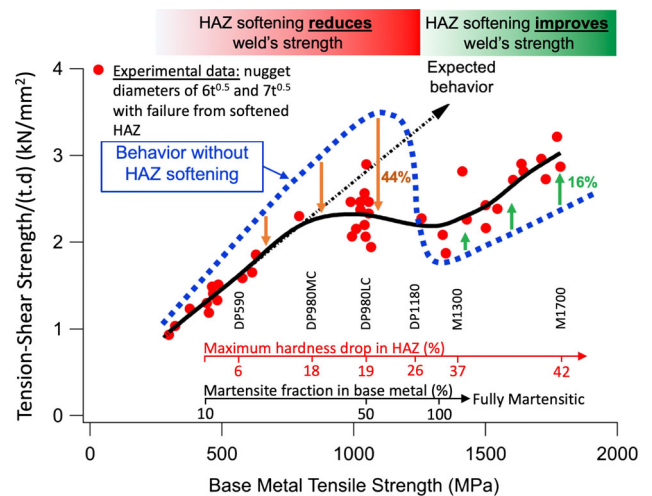


Fig. 9—The complex role of HAZ softening on strength of TS samples made from DP and MS AHSS. While HAZ softening plays a strong role in strength of DP steels and can significantly reduce welds strength, for example by 44 pct in DP980LC sample, depending on the martensite volume fraction in initial microstructure, it has a minor role in strength of MS steels and improves welds strength by 16 pct in M1700 TS sample, as an example. The blue dash-line is from the FE simulations for models for which base metal material properties were used for the softened regions, SCHAZ and ICHAZ.

from our FE simulations showed 44 pct drop in its strength due to HAZ softening in both SCHAZ and ICHAZ of spot weld. As it can be seen, the HAZ softening shows a more significant role in reduction of the strength of spot welds made from DP steels as the initial fraction of martensite increases. This can be related to the fact that the martensite acts as the strengthening (and hardening) micro-constituent in these types of AHSS and as the HAZ softening significantly reduces martensite strength (and hardness) in regions close to the spot weld, it results in a drop in

peak load and global deformation of spot-welded sample made from these DP steels. This trend continues with increase in the volume fraction of hard and brittle martensite and upon reaching to the values perhaps around 80 pct of martensite fraction (corresponding to DP1180), an opposite role of HAZ starts to be noticed. From this point and due to the large amount of hard and brittle martensite in the initial microstructure, base metal shows an intrinsic semi-brittle behavior with low ductility. For instance, total elongation for M1700 fully martensitic steel is about 5 pct. For these steels, the HAZ softening helps with increase in local plastic deformations in softened zones (mainly SCHAZ and ICHAZ), and therefore, more energy can be absorbed by the larger amount of plastic deformations. As a result global extension and load bearing capacity (TSS and CTS) in these steels increases, especially in spot welds with large nugget diameters (above 6 mm in the three nugget diameters used in this study).

Our results from FE simulations also showed that without HAZ softening in steels with above 80 pct martensite, the failure location can also change from softened (SCHAZ and ICHAZ) to hardened region (generally in UCHAZ). This is shown and compared in Figure 10 for DP980LC and M1700 spot welds with 8 mm nugget diameter by considering cases with and without HAZ softening. As it can be seen for both steels the local strain localization and failure type were

affected by existence of HAZ softening. While for DP980LC, the occurrence of HAZ softening reduced the local and thus global strength by inducing strain localization to softened HAZ and promoted failure, for M1700 increased the local and structural ductility and delayed the failure by increasing its ability to absorb more energy through local plastic deformations in SCHAZ and ICHAZ. This improved the strength of M1700 spot weld.

B. Uncertainties in FE Simulation of AHSS Spot Welds

Results shown in previous sections showed that there are differences between results obtained from FE simulations and those from experiments for TS and CT samples. These differences were mainly in peak load (TSS and CTS) and global extension (TSE and CTE) and results for local deformations and failure behaviors were similar. Figures 11(a) and (b) quantitatively summarizes these differences between TSS and CTS values, respectively, for three grades of steel and three nugget diameters used in this study. Failure modes are also shown in this figure.

Steps were taken by adjusting the fracture criteria for different regions of HAZ to calibrate the FE models so that the results match better with those from experiments. As can be seen, as the nugget diameter increases from 4 to 6 and then 8 mm, the difference between

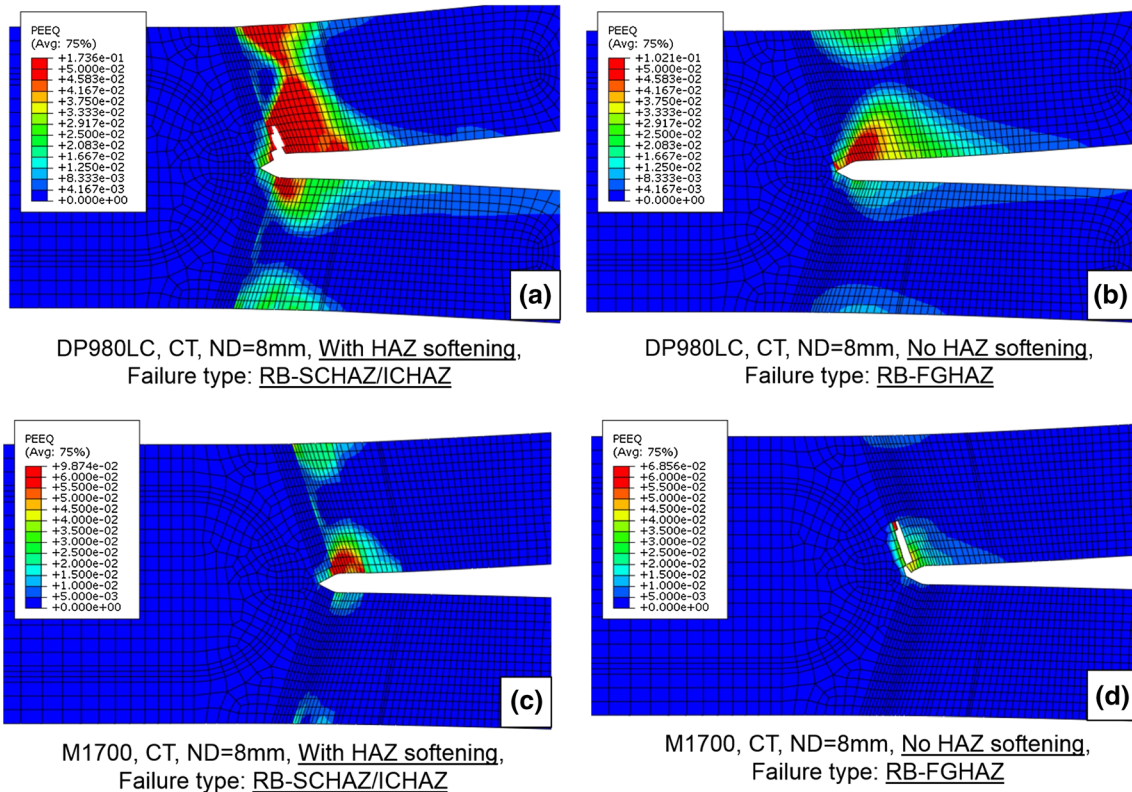


Fig. 10—Equivalent plastic strain localization, crack initiation, and propagation on the cross-section of CT sample made from DP980LC in (a) and (b), and M1700 in (c) and (d), with and without HAZ softening obtained from FE simulations. In DP980LC HAZ softening resulted in premature failure and in M1700 improved the strength of sample. Local and global deformation behavior and failure type and mechanisms are affected by existence of HAZ softening in these samples.

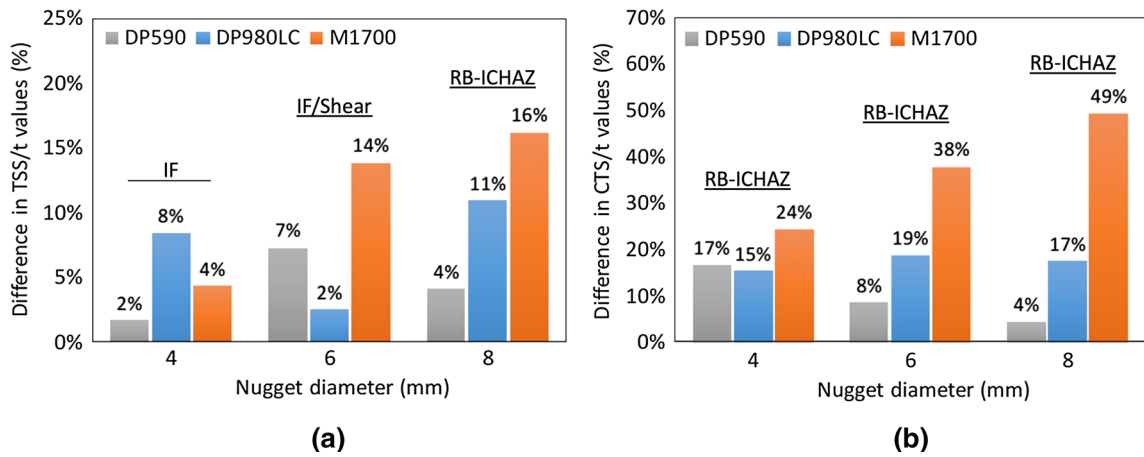


Fig. 11—Calculated difference between the peak loads measured from experiments and those obtained from FE simulations for TS (a) and CT (b) samples with 4, 6, and 8 mm nugget diameters. The difference between results increases from DP590 to DP980LC and then M1700 as the material heterogeneity and nugget diameter increase.

results from FE simulations and experiments increases in both TS and CT samples. This is interesting to notice that in samples with larger nugget diameters failure occurs in the regions where martensite tempering and softening occurs (SCHAZ and ICHAZ). In addition, the differences are larger for CT samples with values up to 49 pct for CT sample with nugget diameter of 8 mm made from M1700 steel. In all the CT samples, the failure mode was RB-ICHAZ. To understand the underlying reasons for these differences there is a need to understand the uncertainties and assumptions relevant to both the TS and CT experiments and FE simulations. Some of these uncertainties are listed in the following and explained later in this section:

1. A stepwise (*vs* continuous) method was used to assign material properties to HAZ regions in FE models.
2. Effects of stress triaxiality and strain rate dependency on constitutive properties and damage model with failure criteria were neglected.
3. Loading fixtures used for TS and CT tests and measurement techniques could impact the results.
4. Existence of fabrication defects such as micro-cracks at the notch tip and formation of voids (porosity) on faying surface and inside the spot welds.
5. Measurement of nugget diameter from TS and CT samples.

1. Material distribution in HAZ

While a continuous material distribution and gradual change between HAZ regions exist in the real spot welds, a stepwise method was used in FE models for TS and CT samples (see Figures 2 and 3). The stepwise method was used in FE simulations due to the limited number of peak temperatures used in Gleeble simulations and thus limited number of available local constitutive properties. In this method, a constant material property is used for a region of HAZ. This, however, does not represent the real material

distribution is spot welds and can be a source of uncertainty in results from FE simulations.

2. Damage model and failure criteria

In this study and as explained in previous sections, a damage model based on equivalent plastic strain at failure was used in FE simulations. This plastic strain at failure was obtained from uniaxial tensile testing. Results from several work by other researchers have shown that the fracture strain can significantly change with the stress triaxiality, Lode angle, and strain rate^[37,38] affecting the strength (peak load) and global extension of TS and CT samples obtained from FE simulations.

3. Effect of fabrication and spot weld defects

Results from scanning electron microscopy (SEM) analysis on the cross section of spot-welded samples (see Figure 12(a) as an example) showed the existence of micro-cracks at the notch area, and also micro-voids on the faying surface of spot welds. To investigate the effect of these fabrication defects on spot welds' performance, we included a crack with a length of 200 μm , as shown in Figure 12(b), typical to those observed in spot welds. The results from FE simulations with and without fabrication defects were then compared and presented in Figure 13.

These results suggest that existence of defects can significantly impact the strength and global deformation of spot welds, as shown as an example for M1700 CT sample with nugget diameter of 4 mm in Figure 13. For this sample, while the failure mode (RB-FGHAZ) did not change by addition of the micro-crack, however, crack initiated from a different location and propagated into regions closer to the center of spot weld. In the model with micro-crack, the crack moved towards the nugget and changed path when faced the CGHAZ and continued propagation on the boundary between the FGHAZ and CGHAZ. A comparison between the global load-extension curves for the above two FE models showed that although the failure mode did not

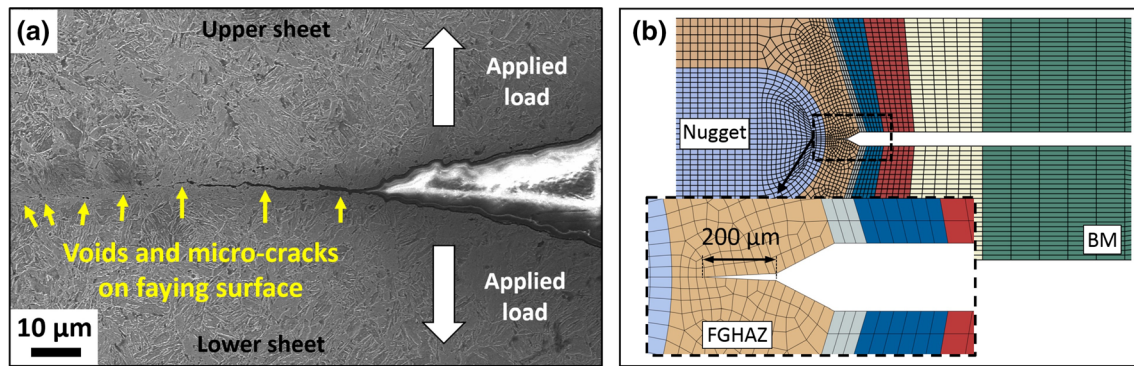


Fig. 12—Results from scanning electron microscopy revealed pre-existence of micro-cracks and voids at the notch tip and on faying surface of the spot welds (a). FE model shown in (b) with and without crack at faying surface for M1700 CT with 4 mm nugget diameter was used to investigate the effect of above defects on mechanical performance of AHSS spot welds.

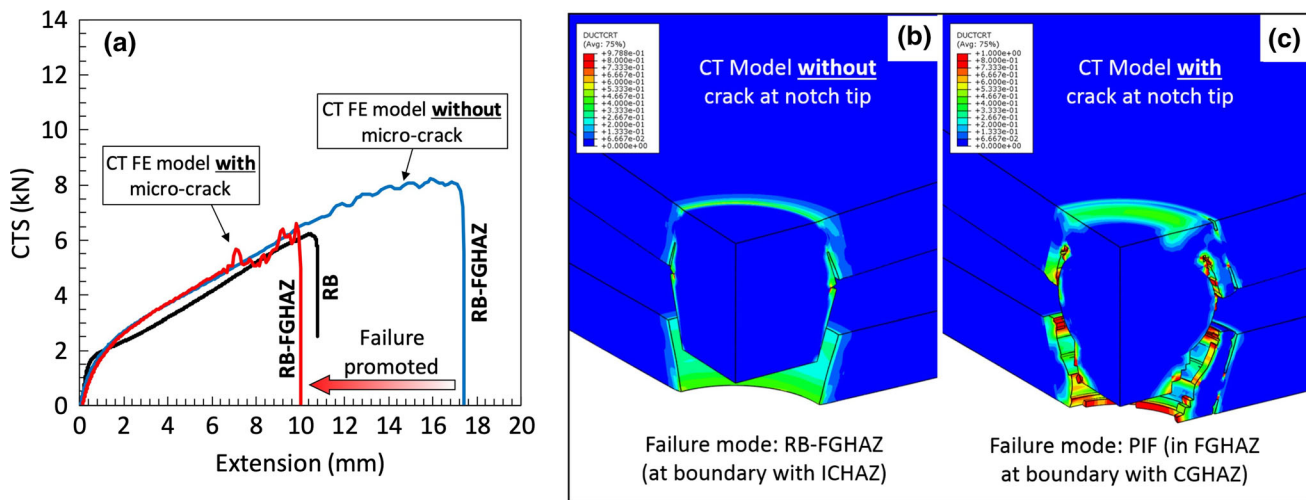


Fig. 13—Results from FE simulation of M1700 CT sample with nugget diameter of 4 mm for the sample with (b) and without (c) micro-crack at the notch tip. Including the micro-crack to model resulted into 28 and 43 pct decrease in peak load and extension at peak load as shown in (a). This also affected the crack path by moving it to regions closer to the nugget for the sample with micro-crack (b).

change, the peak load (CTS) and global extension at peak load in the model with micro-crack decreased by 28 and 43 pct, respectively. This significant change in results should be considered when comparing the results from TS and CT experiments with those from FE simulations, as a source of uncertainty.

VI. CONCLUSIONS

In this work, the complex role of HAZ softening in SCHAZ and ICHAZ and its relationship with the nonlinearity seen in the strength of AHSS spot welds was investigated using the results from FE simulations and tension-shear and cross-tension experiments. Following conclusions can be made based on the results obtained from this study:

1. Results from experiments and FE simulations reconfirmed that the strength of the AHSS spot welds does not increase linearly with their base

metals' strength and/or nugget diameter. Among the material and nugget diameters used in this study, the critical BMS and ND of 980 MPa and 6 mm, respectively, were observed as the values that failure mode changed in both TS and CT samples from a semi-brittle (IF and RB-UCHAZ, also Shear) to a ductile failure (RB-ICHAZ/SCHAZ).

2. Results also suggested that the degradation in local material properties in SCHAZ and ICHAZ, and change in failure mode by increasing in nugget diameter are responsible for the lower strength of spot welds (TSS and CTS) in samples with critical nugget diameters and base metal strength above the critical values.
3. FE simulations showed that with the minimum yield stress belonging to the ICHAZ, the plastic strain localization and failure occurs in this region for spot welds with ND of 8 mm, in all the steels of this study. Results from FE simulations of this study also suggested that improving the resistance

to softening in the SCHAZ cannot be effective until the properties for ICHAZ are improved as well.

4. Experiments and FE simulations showed that the mechanical performance of AHSS spot welds is influenced by the weld geometry and the heterogeneous distribution of constitutive properties in the spot weld. The HAZ softening showed to have a complex role in performance of spot welds. Results from FE simulations showed that HAZ softening can play a different role in different grades of AHSS steels. It was shown that it can result in degradation of strength in DP980LC spot welds while improving M1700 spot weld performance.
5. The uncertainties in experiments and FE simulations were shown to have significant impact on the peak load and global extension of spot-welded samples making it difficult to obtain an accurate assessment of spot weld performance in terms of peak load and extension at peak load from the FE simulations. These models, however, can help in understanding the local–global deformation and failure behavior relationship, as well as the role of individual regions of heat-affected zone of spot-welded samples, as presented in this paper.

ACKNOWLEDGMENTS

The authors of this paper would like to acknowledge the financial support from ArcelorMittal Global R&D for carrying out this research. The authors would like to thank Dr. Shrikant P. Bhat from ArcelorMittal Global R&D for the helpful discussions related to the mechanical performance of AHSS.

REFERENCES

1. H. Rezaayat, H. Ghassemi-Armaki, S.P. Bhat, S. Sriram, and S.S. Babu: *J. Mater. Sci.*, 2019, vol. 54, pp. 5825–43.
2. H. Rezaayat, S. S. Babu and H. Ghassemi-Armaki: in *Trends in Welding Research: Proceedings of the 10th International Conference*, 2016.
3. H. Ghassemi-Armaki, S. Bhat, S. Kelley, and S. Sadagopan: *Weld. J.*, 2017, vol. 96, pp. 104s–112s.
4. H. Ghassemi-Armaki, E. Biro, and S. Sadagopan: *ISIJ Int.*, 2017, vol. 57, pp. 1451–60.
5. E. Biro, J.R. McDermid, S. Vignier, and Y.N. Zhou: *Mater. Sci. Eng. A*, 2014, vol. 615, pp. 395–404.
6. E. Biro, S. Vignier, C. Kaczynski, J.R. McDermid, E. Lucas, J.D. Embury, and Y.N. Zhou: *ISIJ Int.*, 2013, vol. 53, pp. 110–18.
7. G. Krauss and A.R. Marder: *Metall. Trans.*, 1971, vol. 2, pp. 2343–57.
8. E. Biro, J.R. McDermid, J.D. Embury, and Y. Zhou: *Metall. Mater. Trans. A*, 2010, vol. 41A, pp. 2348–56.
9. V.H.B. Hernandez, S.S. Nayak, and Y. Zhou: *Metall. Mater. Trans. A*, 2011, vol. 42, pp. 3115–29.
10. V.H.B. Hernandez, S.K. Panda, Y. Okita, and Y.N. Zhou: *J. Mater. Sci.*, 2009, vol. 45, pp. 1638–47.
11. E. Biro, J.R. McDermid, J.D. Embury, and Y. Zhou: *Metall. Mater. Trans. A*, 2010, vol. 41, pp. 2348–56.
12. M. Xia, E. Biro, Z. Tian, and Y.N. Zhou: *ISIJ Int.*, 2008, vol. 48, pp. 809–14.
13. N. Yamauchi, T. Taka, K. Kunishige, and N. Nagao: *Iron Steel Inst. Jpn.*, 1982, vol. 22, p. B107.
14. E. Biro, S.S. Nayak and Y. Zhou: in *Trends in Welding Research: Proceedings of the 9th International Conference*, 2013, pp. 201–07.
15. S. Vignier, E. Biro, and M. Herve: *Weld. World*, 2014, vol. 58, pp. 297–305.
16. S. Dancette, D. Fabregue, R. Estevez, V. Massardier, T. Dupuy, and M. Bouzekri: *Eng. Fract Mech.*, 2012, vol. 87, pp. 48–61.
17. S. Dancette, D. Fabregue, V. Massardier, J. Merlin, T. Dupuy, and M. Bouzekri: *Eng. Fract Mech.*, 2011, vol. 78, pp. 2259–72.
18. S. Dancette, D. Fabregue, V. Massardier, J. Merlin, T. Dupuy, and M. Bouzekri: *Eng. Fail. Anal.*, 2012, vol. 25, pp. 112–22.
19. M. Bouzekri, S. Dancette, V. Massardier, D. Fabregue, and H. Klocker: *Weld. World*, 2010, vol. 54, pp. 3–14.
20. S.S. Nayak, Y. Zhou, V.H.B. Hernandez, and E. Biro: in *Trends in Welding Research: Proceedings of the 9th International Conference*, 2013, pp. 641–49.
21. M. Pouranvari and S.P.H. Marashi: *Mater. Sci. Eng. A*, 2011, vol. 528, pp. 8337–43.
22. Y.P. Yang, S.S. Babu, F. Orth, and W. Peterson: *Sci. Technol. Weld. Join.*, 2008, vol. 13, pp. 232–39.
23. M. Tamizi, M. Pouranvari, and M. Movahedi: *Sci. Technol. Weld. Join.*, 2017, vol. 22, pp. 327–35.
24. T. Huin, S. Dancette, D. Fabregue, and T. Dupuy: *Metals*, 2016, vol. 6, p. 111.
25. X. Wang, C. Sun, and A. Dai: *Materials*, 2019, <https://doi.org/10.3390/ma12060900>.
26. K. Paveebunvipak and V. Uthaisangasuk: *Mater. Des.*, 2018, vol. 160, pp. 731–51.
27. K. Paveebunvipak and V. Uthaisangasuk: *J. Mater. Eng. Perform.*, 2019, vol. 28, pp. 2017–28.
28. H. Rezaayat, H. Ghassemi-Armaki, S. P. Bhat, S. Sriram, and S. S. Babu: *J. Mater. Eng. Perform.*, 2020.
29. Y.J. Chao: *Sci. Technol. Weld. Join.*, 2003, vol. 8, pp. 133–37.
30. K. Perzynski, A. Wroczynka, R. Kuziak, A. Legwand, and L. Madej: *Finite Elem. Anal. Des.*, 2017, vol. 124, pp. 7–21.
31. ASTM standard E8M: *Tension Testing of Metallic Materials*, ASTM International, West Conshohocken, PA, 1998.
32. ASTM standard E3-01: *Standard Practice for Preparation of Metallographic Specimens*, ASTM International, West Conshohocken, PA, 2001.
33. Michael Smith: *ABAQUS Documentation*, Dassault Systèmes, Providence, RI, 2011.
34. American Welding Society: AWS/SAE D8.9 M: Recommended practices for test methods for evaluating the resistance spot welding behavior of automotive sheet steel materials, 2012.
35. H.G. Koenigsberger: *Am. Hist. Rev.*, 1977, vol. 82, pp. 946–48.
36. G.B. An, S.K. Nam, and T.W. Jang: *Mater. Sci. Forum*, 2008, vols. 580–582, pp. 589–92.
37. C.C. Tasan, M. Diehl, D. Yan, C. Zambaldi, P. Shanthraj, F. Roters, and D. Raabe: *Acta Mater.*, 2014, vol. 81, pp. 386–400.
38. C.C. Tasan, J.P.M. Hoefnagels, M. Diehl, D. Yan, F. Roters, and D. Raabe: *Int. J. Plast.*, 2014, vol. 63, pp. 198–210.

Publisher's Note Springer Nature remains neutral with regard to jurisdictional claims in published maps and institutional affiliations.